In vivo selective cancer-tracking gadolinium eradicator as new-generation photodynamic therapy agent

Tao Zhang[a,b], Rongfeng Lan[a], Chi-Fai Chan[a], Ga-Lai Law[c,1], Wai-Kwok Wong[a,1], and Ka-Leung Wong[a,1]

[a]Department of Chemistry and State Key Laboratory of Environmental and Biological Analysis, Hong Kong Baptist University, Kowloon Tong, Hong Kong SAR; [b]Ministry of Education Key Laboratory of Laser Life Science & Institute of Laser Life Science, College of Biophotonics, South China Normal University, Guangzhou 510631, People's Republic of China; and [c]Department of Applied Biology and Chemical Technology, The Hong Kong Polytechnic University, Hung Hom, Hong Kong SAR

Edited by Kenneth N. Raymond, University of California, Berkeley, CA, and approved November 6, 2014 (received for review August 6, 2014)

In this work, we demonstrate a modality of photodynamic therapy (PDT) through the design of our truly dual-functional—PDT and imaging—gadolinium complex (Gd-N), which can target cancer cells specifically. In the light of our design, the PDT drug can specifically localize on the anionic cell membrane of cancer cells in which its laser-excited photoemission signal can be monitored without triggering the phototoxic generation of reactive oxygen species—singlet oxygen—before due excitation. Comprehensive in vitro and in vivo studies had been conducted for the substantiation of the effectiveness of Gd-N as such a tumor-selective PDT photosensitizer. This treatment modality does initiate a new direction in the development of "precision medicine" in line with stem cell and gene therapies as tools in cancer therapy.

gadolinium | imaging | in vivo PDT | survivin | tumor recognition

Significant challenges of tumor cells recognition, in-depth light penetration, and in situ monitoring are confronted by scientists to develop photodynamic therapy (PDT) as a reliable clinical treatment for cancers (1, 2). To address the penetration depth and molecular imaging issues, the utilization of near-infrared (NIR) excitation (via multiphoton/up-conversion processes) and emission within the "biological windows" (such as first window: 600–950 nm; second window: 1–1.35 μm; and third window: 1.5–1.8 μm) (3) has provided a satisfying resolution because NIR photons can penetrate deep into the tissue and reemit sharply without being absorbed by the cell even in the blood media and causing damage. Clear images can be obtained and differentiated then from the usual biological autofluorescence background (4). Recently, two-photon absorption photodynamic therapy (TPA-PDT) has received increasing attention (5). Porphyrin-based photosensitizers are considered as the prime candidates as their two-photon (TP)–induced singlet oxygen ($^1O_2$) generation and red/NIR emission (~650 and ~750 nm) are very efficient and intense. Several design strategies for TPA-PDT photosensitizers have been reported in the literature, but only very few of those compounds are tumor cell-specific or have been investigated in vitro and in vivo, concerning especially porphyrins and lanthanides (6). For instance, selective closure of blood vessels through two-photon excitation PDT in vivo using porphyrin dimers of large TP absorption cross-section has been demonstrated currently (7); tumor selectivity of amphiphilic photosensitizers has also been found related to their efficient binding to low-density lipoproteins, which are responsible for the transport of porphyrins to tumor tissues (8, 9). High–molecular-weight porphyrins, in essence, preferentially accumulate on solid tumors and are expected to be internalized into membrane-limited organelles, thereby achieving controlled localization in the intercellular compartment (10). However, it has still been arduous for PDT probes to come into contact with cancer cells in particular, with two major problems being associated with commercially available or literature-reporting photosensitizers for photodynamic treatment: (*i*) the recognition of cancer cells and (*ii*) the monitoring of their effectiveness. In this regard, we had reported previously a specific phospholipid marker—an ytterbium-porphyrin complex (Yb-N), which has a strong binding with anionic phospholipid species in solution and can identify several of them in a number of cancer cells via long-lived visible-to-NIR lanthanide luminescence (11). A limitation of this complex is that it does not photogenerate $^1O_2$. Without the advances in stem cell and gene therapy against cancers for 100% efficiency, it is always essential to explore any potential alternative methodology for the sake of human well-being. Herein, we present our newly developed gadolinium porphyrinate (Gd-N), a potential PDT agent, which had been synthesized on the basis of Yb-N and shown 51% singlet oxygen quantum yield with characteristic NIR emission of the porphyrin upon photoexcitation (Fig. 1*A*). Comprehensive studies of it have revealed that Gd-N can recognize tumor cells by their anionic phosphotidylserine membrane in the first six dosed hours and that, upon administration of laser irradiation at certain wavelengths, it can enter the tumor cells and produce $^1O_2$ in addition to exhibiting TP-induced NIR emission. Results of the in vivo mouse models and biodistribution assays have further illustrated that Gd-N was found to be located in the tumor after simple injection of Gd-N into the blood vessel. Upon $^1O_2$ releasing from the porphyrin, the solid tumor was found to be reduced after 24-h treatment. To the best of our knowledge, there is a dearth of examples of in vivo lanthanide-based PDT agents in the literature. Our Gd-N can, therefore, serve as a blueprint for the development of next-generation smart PDT agents with the use of lanthanide porphyrinates for practical cancer tracking, imaging, and killing.

Significance

Next-generation photodynamic therapy (NG-PDT) for the treatment of tumors preponderates over conventional practices in that it is a kind of effective precision medicine with minimal invasive procedures and side effects. Herein, a newly developed NG-PDT paradigm agent of gadolinium-porphyrin complex, Gd-N, is introduced, which can successfully trace and recognize tumor tissues via simple injection into the blood vessel of the mouse models, selectively accumulate within them, and superiorly exert the therapeutic effect via cytotoxic singlet oxygen generation (~51% quantum yield) to eradicate the solid tumor by one-half within a short period of time only upon due two-photon excitation. Its characteristic two-photon–induced near-infrared emission is also always available for direct monitoring for transportation and effectiveness in vitro and in vivo.

Author contributions: W.-K.W. and K.-L.W. designed research; T.Z., R.L., C.-F.C., G.-L.L., W.-K.W., and K.-L.W. performed research; T.Z., G.-L.L., W.-K.W., and K.-L.W. contributed new reagents/analytic tools; T.Z., R.L., C.-F.C., G.-L.L., and K.-L.W. analyzed data; and T.Z., R.L., G.-L.L., W.-K.W., and K.-L.W. wrote the paper.

The authors declare no conflict of interest.

This article is a PNAS Direct Submission.

Freely available online through the PNAS open access option.

[1]To whom correspondence may be addressed. Email: klwong@hkbu.edu.hk, wkwong@hkbu.edu.hk, or ga-lai.law@polyu.edu.hk.

This article contains supporting information online at www.pnas.org/lookup/suppl/doi:10.1073/pnas.1414499111/-/DCSupplemental.

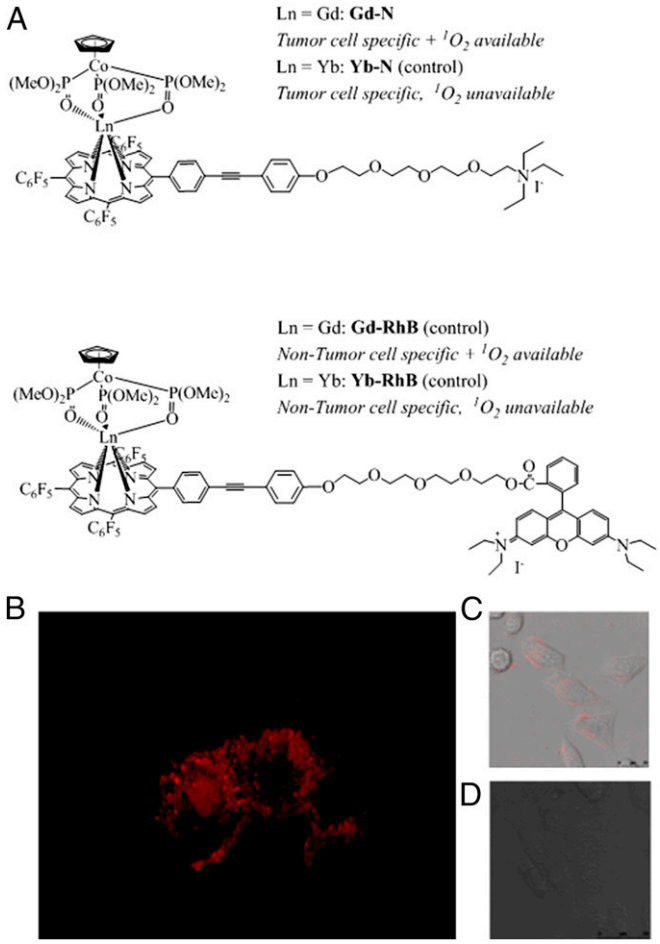

Fig. 1. (*A*) The molecular structure of our smart cancer cells-specific photodynamic therapy agent (Gd-N) and their control analogs Yb-N and Gd-RhB. (*B*) The 3D in vitro imaging of Gd-N after 15-h incubation in HeLa cells [see 3D movie (Movie S1)]. (*C* and *D*) The difference in subcellular localization of Gd-N in cancer cells (HeLa) and normal cells (WPMY-1).

Results and Discussion

The detailed synthesis and characterization of Gd-N, which is the motif structure of our ytterbium complex (Yb-N) reported in our previous work, can be found in *SI Text* (Scheme S1 and Fig. S1). Gd-N and Yb-N are structurally more or less identical (the vector ligated to Gd-N is also the same as Yb-N), except for the lanthanide ion present in the complex. It is self-evident that porphyrin's coordination with different lanthanides can cause changes in not merely the NIR emission from itself, yet also the $^1O_2$ generation simultaneously (Fig. 2 and Fig. S2). Such phenomena, in principle, can arise from better orbital overlapping between the metal center resulting in better energy transfer (i.e., the bonding orbitals of Yb, which consists of a smaller atomic radius than Gd, thus overlap more preferably and compatibly with the porphyrin's orbitals). The heavy-atom effect exerted by the lanthanide can enhance the triplet-state decay rate and lead to higher triplet-state quantum yields of the porphyrin system (12). According to the spectroscopic studies, the singlet oxygen quantum yield of Yb-N was measured to be 0% and Gd-N was determined to be 51%. The calculations were based on (*i*) the NIR phosphorescence intensity of the $^1O_2$ (at 1,270 nm) produced from the two complexes and (*ii*) the lowest excited states of ytterbium $^2F_{5/2}$ (~10,200 cm^{-1}) and gadolinium $^6P_{7/2}$ (~32,000 cm^{-1}), respectively. It should be noted that the latter energy level of $^6P_{7/2}$ is much higher than the singlet/triplet levels of the porphyrin unit (singlet states, ~23,200 and 15,300 cm^{-1}; triplet state, 12,500 cm^{-1}). An assumption has it that, for such a large energy gap between porphyrin and Gd, there is no energy transfer from porphyrin to Gd; the energy gained can therefore purely be either dissipated in the form of light or used to form singlet oxygen, making direct determination of $^1O_2$ quantum yield feasible (Fig. S3*A*) (13–15). This is entirely not the same case for Yb. As the energy gap between porphyrin and Yb is small, most of the energy absorbed by the porphyrin unit would just be simply transferred to the ytterbium efficiently (via heavy-atom effect) and afford the characteristic *f-f* emission exclusively (Fig. S3*B*). The two percentages have clearly shown that nearly one-half part of the energy absorbed by the porphyrin of Gd-N would be involved in the $^1O_2$ generation, whereas the rest will be normally used for the porphyrin's NIR emissions; in contrast, for Yb-N, ytterbium's *f-f* luminescence at 1.08 μm is the dominant process of energy consumption under the same photoexcitation (linear and two-photon excitation at 430 and 860 nm, respectively; the two-photon absorption cross-section of Gd-N and Yb-N are similar in being ~351 GM; Fig. S4).

Investigations with relation to real PDT applications of Gd-N in vitro and, particularly, in vivo had been accomplished in terms of tumor selectivity, cytotoxicity and photocytotoxicity, imaging, PDT efficiency, as well as biodistribution. The selectivity of Gd-N against tumor and normal cells are superiorly distinct. As shown in Fig. 1 *B–D*, in the HeLa cancer cell, strong red emission from the porphyrin of Gd-N can be observed on the periphery, that is, the membrane surface, after 2-h incubation; upon incubation with more than 15 h, several red emission can even enter and scatter internally to the cytoplasm. [Please refer to the 3D movie (Movie S1).] In the normal cell MRC-5, however, no emission can be detected on the surface of or inside the cell even after the 12 h of incubation. To have a fair comparison, Gd-RhB had been synthesized for the control experiments. Rhodamine B (RhB) is a well-known mitochondria vector common for conjugation. Under the same experimental condition (incubation time, concentration, cell lines, and laser power), we can find Gd-RhB's emission in both normal and cancer cells' mitochondria, and this very observation becomes the clear, cognizant, and convincing evidence of the tumor-specific property of our Gd-N (Fig. 3). Through the 3-(4,5-dimethylthiazol-2-yl)-2,5-diphenyltetrazolium bromide (MTT) assays, the cytotoxicity of the three complexes, Gd-N, Yb-N, and Gd-RhB, in dark can be subsequently determined against the two kinds of cell lines. The IC_{50} values of them are 0.78, 0.80, and 0.65 mM in cancer cells (HeLa) and 0.70,

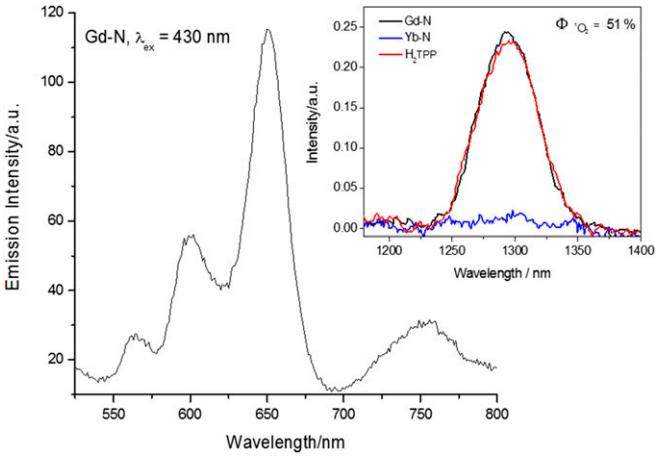

Fig. 2. The emission spectra of Gd-N (HEPES buffer solution, 10 μM, λ_{ex} = 430 nm, pH 7.4) and $^1O_2$ quantum yield measurement. [NIR phosphorescence spectra of $^1O_2$, $CHCl_3$, 10 μM, λ_{ex} = 430 nm, abs(λ_{ex}) = 0.03; Yb-N is the control and tetraphenylporphyrin (H2 TPP) is the standard for $^1O_2$ measurement (11).]

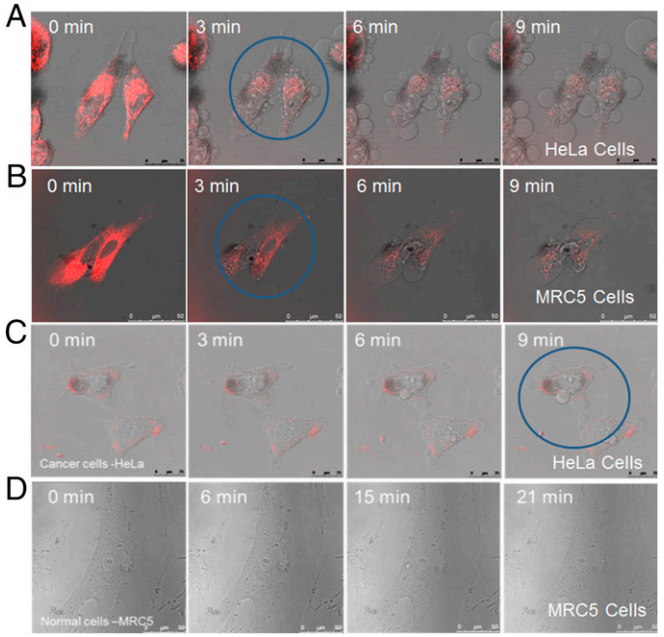

Fig. 3. The in vitro imaging of Gd-N and Gd-RhB in tumor cells, HeLa, and normal cells, MRC5 (as the controls) after 2-h incubation. PDT effect was triggered upon 860-nm excitation. (*A*) Gd-RhB in HeLa. (*B*) Gd-RhB in MRC-5. (*C*) Gd-N in HeLa. (*D*) Gd-N in MRC-5 (1 μM).

0.70, and 0.45 mM in normal cells (MRC-5), respectively. The underlying reason of the vast difference in the dark cytotoxicity of Gd-RhB toward cancer/normal cells compared with the other two can be largely due to its nonselectivity. Again, it is the peculiarity of our Gd-N that makes possible this crucial tumor selectivity. The in vitro PDT effect of the three complexes was evaluated using in vitro confocal microscopy and photocytotoxicity assays. Gd-N, Yb-N, and Gd-RhB complexes had been dosed in HeLa cells and MRC-5 cells for 6 h, and then subjected to excitation at 860 nm for triggering any PDT effect. (Three complexes are all available for TP-induced in vitro imaging with TP cross-section ~351 GM; given the limitation of our confocal spectroscope, the emission from porphyrin had only been monitored from 600 to 750 nm.) In Fig. 3, the emission of Gd-RhB can be noticed in the mitochondria. Upon suitable laser induction, only small quantities of $^1O_2$ can be produced, but the cancer cells can be killed within a few minutes; in effect, the normal cells can also be killed rapidly under the same conditions. The PDT effect of Gd-RhB is therefore efficient enough but obviously undesirable; it can accumulate inside the mitochondria of cancer and normal cells, annihilating them unselectively. Although Yb-N is cancer specific, its incapability to produce any $^1O_2$ imposes a restriction on its any PDT practice. Surprisingly, when it comes to our red emissive Gd-N, not only can it recognize and localize on the anionic membrane of the tumor cell, but it can also get access to certain parts of the cytoplasm and induce cancer apoptosis via $^1O_2$ upon 9-min light dose flashing 5 s per minute. Of course, it is very true that more time is required to trigger cancer cell deaths by Gd-N after definite laser irradiation; however, there are no significant cell deaths in the normal cells that far outweigh its slow-response drawback.

As any new-generation PDT agent, the concentration-dependent photocytotoxicity of Gd-N, Yb-N, and Gd-RhB, ranging from 0.2 to 1 μM dosage, had also been measured under varying light doses from 0.25 to 1 J/cm^2 in cancer cells and normal cells. The light dose–response curves obtained are displayed in Fig. 4*A*. In the HeLa cancer cells, Gd-RhB and Gd-N have exhibited strong photocytotoxicity, whereas Yb-N (without singlet oxygen) has no photocytotoxicity. From Fig. 4*B*, in the normal cell QSG-7701, no photocytotoxicity can be found from Gd-N, whereas Gd-RhB gives very similar results to its behavior in the cancer cells. Such a trend does seem to correlate with the selective cellular uptake of Gd-N by the cancer and normal cells. We had extended the studies with the use of more cancer cell and normal cell lines, and the results are shown in Fig. 5—Gd-N can maintain its good tumor selectivity toward a total of seven cell lines (four cancer cells and three normal cells), thereby acting as an outstanding and specific PDT agent.

To understand more about the in vivo uptakes of our complexes, studies of biodistribution on our complexes' specialty toward particular organs infections had been carried out via xenograft mouse models and inductively coupled plasma mass spectrometry (ICP-MS) (16). In the first proof-of -concept experiment, the four complexes had been classified into four groups. HeLa cells pre-incubated separately with Gd-N, Yb-N, Gd-RhB, and Yb-RhB were s.c. injected into BALB/c nude mice, and then the injected sites were irradiated with 860 nm laser. Two weeks later, mice were

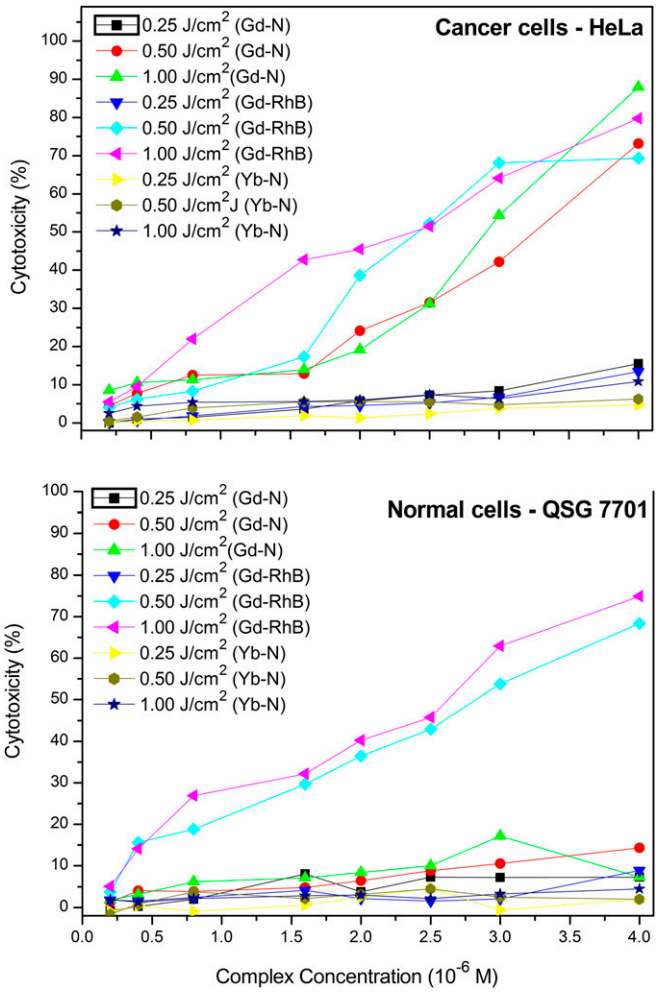

Fig. 4. The photocytotoxicities of Gd-N, Gd-RhB (control), and Yb-N (control) towards the cancer cell (*A*, HeLa) and normal cell (*B*, QSG 7701). Gd-N ($^1O_2$ available, tumor specific, strong photocytotoxicity in cancer cells, but no photocytotoxicity in normal cells), Gd-RhB (control, $^1O_2$ available, nontumor specific, strong cancer and normal cell photocytotoxicity), and Yb-N (control, $^1O_2$ not available, no photocytotoxicity in both cancer and normal cells). Photocytotoxicity curves were obtained using 1 μM of conjugates and various light doses from 0 to 1 J/cm^2; MTT assays were carried out after incubation for 24 h (37 °C, 5% CO_2).

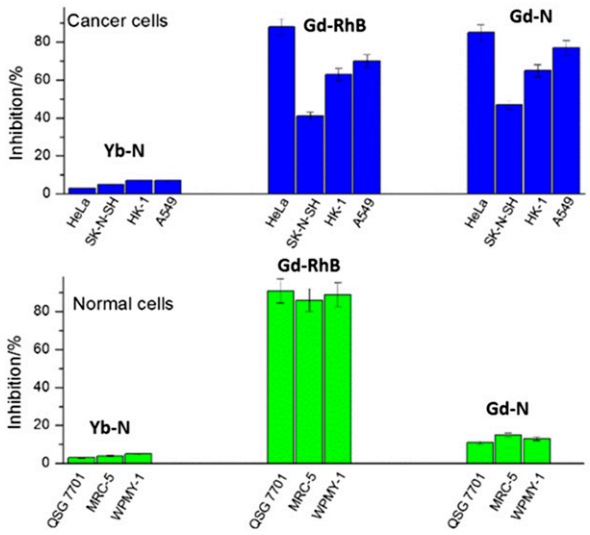

Fig. 5. The in vitro photocytotoxicity assays (λ_{ex} = 430 nm) of our tumor-specific Gd-N in four tumor cell lines (HeLa, SK-N-SH, HK-1, and A549) and three normal cell lines (QSG 7701, MRC-5, WPMY-1), as well as the two controls, Yb-N and Gd-RhB.

pictured and the tumor volumes were measured (Fig. 6 *A* and *B*) and the tumors were found much effectively inhibited in the groups of Gd-N and Gd-RhB, compared with their counterparts Yb-N and Yb-RhB; Gd-N, among the four complexes, is the best in vivo PDT agent that can devastate the tumor with 100% efficiency. Biodistribution study-wise, BALB/c nude mice with tumor xenograft attaining a size of ~0.1 cm^3 were caudal vein injected with Gd-N (1.0 mg/kg). Two days after the chemical administration, the concentrations were examined using ICP-MS. It is tumors that have the largest enrichment of Gd-N (4.84 ppm/g) that suggest the specific recognition of our Gd-N toward tumor cells (Fig. 6*C*).

This result was also confirmed by two-photon microscopic imaging of the tumor tissues extracted from Gd-N–administered BALB/c nude mice (Fig. 6*D*). Further verification of the inhibiting effect of Gd-N and Gd-RhB toward tumor growth in tumor-bearing mice was done by intratumorally injecting BALB/c nude mice of HeLa xenograft tumor of ~0.3 cm^3 with, respectively, Gd-N (2.0 mg/kg), Gd-RhB (2.0 mg/kg), and 5-aminolevulinic acid (ALA) (60 mg/kg) (which can produce protoporphyrin in living cells and herein serve as the control PDT chemical), and irradiating with 860-nm light for 3 h after complex injection (17). The total light dosage to tumor was 50 J/cm^2. Tumors were then allowed for growth for another 7 d and subjected for final extraction and picturing. The outcomes of these studies do constitute that Gd-N is capable of tremendously inhibiting and even reducing the size of solid tumor by one-half from 2 to 1 cm within a short period (Fig. 6*E*).

Alternatively, mice with xenograft tumor were caudal vein injected with Gd-N and Gd-RhB (2.0 mg/kg body weight) and allowed for full circulation for 6 h. Then tumors were irradiated with 860-nm light similarly as above. The tumor on the opposite side served as the control (light untreated). The treatments were repeated for three times in the following days in a one-time-per-day manner. Consistently, we had found that Gd-N-plus-light–treated tumors were inhibited compared with their opposite flank controls of tumor or Gd-RhB groups. Pharmacokinetics analyses also showed that Gd-N persisted in animals for a longer time with a larger mean residence time (MRT) value (8.66 h), whereas Gd-RhB was fast cleared (with MRT of 3.49 h) (Fig. 6*F* and Table S1).

In regard to the molecular mechanism of PDT, the protein levels of cellular survivin and inhibitors of apoptosis protein family (IAP) in protein lysates of PDT-treated HeLa cells were also investigated (18). As proposed, survivin and the IAP family members, c-IAP1, c-IAP2, and XIAP, were all well expressed in Gd-N-plus-laser–treated samples. It is rather surprising to find that mTOR pathway may be involved in response to the PDT treatment of the cancer cells. The levels of two critical members, mTOR and GβL, were also obviously elevated upon Gd-N– or Gd-RhB–induced $^1O_2$ stress stimulus. These results demonstrate the successful cell killing effect of Gd-N promoted PDT at the molecular level and may also shed new light on the design and improvement of current PDT agents (Fig. 7).

Conclusion

Our newly developed theranostic gadolinium complex Gd-N does have great potential to serve as an anticancer agent that is equipped with visible-to-NIR emission for imaging, tumor cell selectivity, and $^1O_2$ generation. Through a string of in vitro and in vivo studies, we believe that the effectiveness and advantages of our Gd-N had been adequately corroborated and demonstrated that our Gd-N lends itself to being a potential next-generation smart dual-functional PDT agent. Our proposed work here can be promising for the development of long-term live cancer cell tracking and imaging, as well as modern practices of selective PDT.

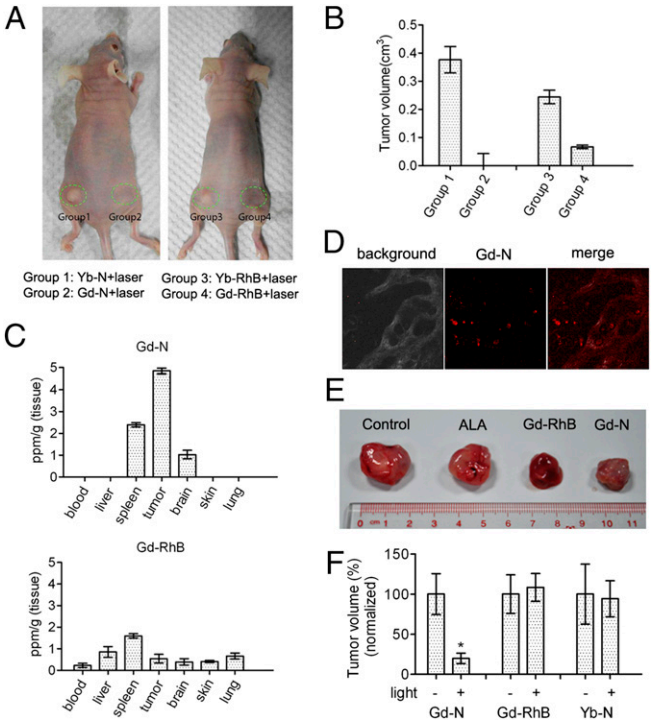

Fig. 6. In vivo studies of Gd-N as the cancer cell-specific PDT agent. (*A*) The representative gross images of tumors after PDT using 860-nm laser for excitation, and candidates were divided into four groups (group 1: Yb-N; group 2: Gd-N; group 3: Yb-RhB; group 4: Gd-RhB). (*B*) The measurement of tumor volume in *A*. (*C*) In vivo biodistribution of Gd-N via ICP-MS studies. (*D*) Two-photon microscopic images of tumor samples in *C*. (*E*) In vivo tumor inhibition assays of Gd-N. Experimental conditions are described in the text. (*F*) In vivo tumor inhibition via Gd-N– and Gd-RhB–induced $^1O_2$ through caudal vein injection.

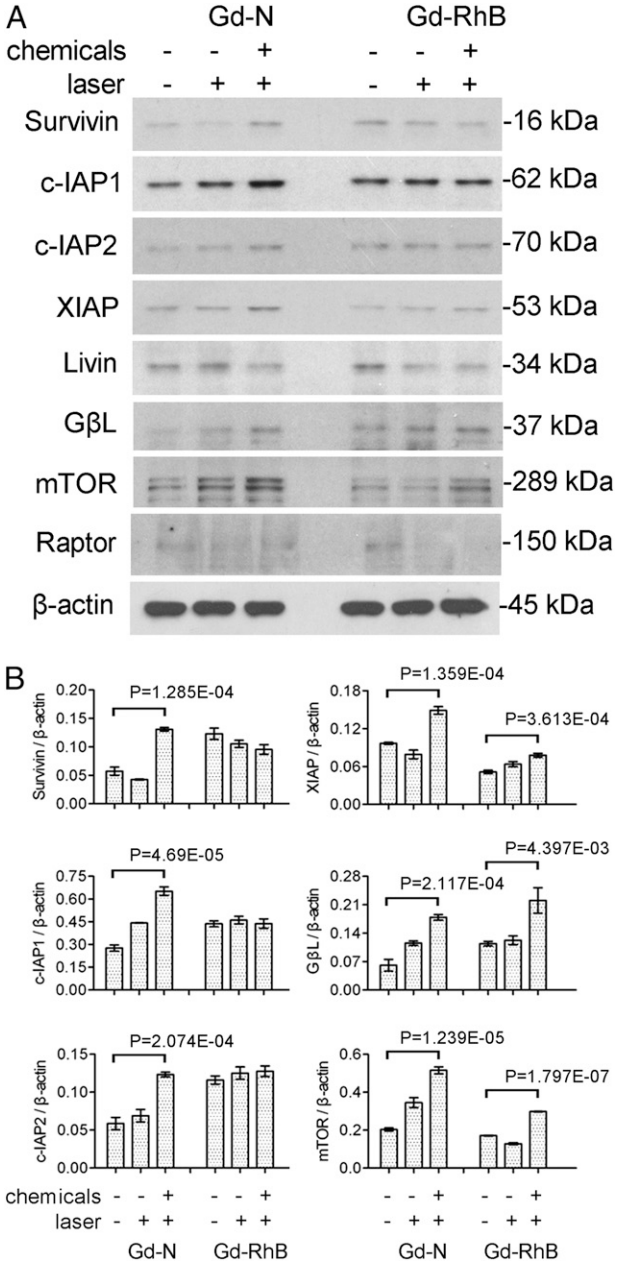

Fig. 7. Gd-N– and Gd-RhB–induced $^1O_2$ activated the inhibitor of apoptosis protein family and mTOR pathway. (*A*) HeLa cells dosed with 1 μM Gd-N or Gd-RhB and irradiated with 0.5 J/cm^2 were harvested for Western blotting. Untreated or free-of-chemicals samples served as the controls. (*B*) Cellular protein changes were semiquantitatively measured using Gel-Pro Analyzer software of Western blotting bands in *A* and showed as the ratio to β-actin (loading control of total proteins). *P* values were calculated between untreated and Gd-N or Gd-RhB plus laser groups by one-way analysis of variance.

Methods

Linear Induced Photophysical Properties. We had recorded the UV–visible absorption spectra (ranging from 200 to 1,100 nm) and single-photon luminescence spectra of all our complexes with, respectively, an HP UV-8453 spectrophotometer and an Edinburgh Instrument FLS920 Combined Fluorescence Lifetime and Steady-State Spectrophotometer equipped with a UV-to-NIR–sensitive photomultiplier inside a nitrogen flow cooled housing. We had corrected all of the spectra from the detector response and stray background light phosphorescence, measuring the quantum yields of the lanthanide complexes by a demountable 142-mm (inner) diameter barium sulfide-coated integrating sphere supplied with the two access ports in Edinburgh Instrument FLS920.

Singlet Oxygen Quantum Yield. With the phosphorescence at 1,270 nm, we had detected the singlet oxygen with an InGaAs detector on the PTI QM4 luminescence spectrometer, and determined the quantum yields (Φ_Δ) of all compounds in $CHCl_3$ through comparing the $^1O_2$ emission intensity of the sample solution to that of a reference material (4) (H_2TPP, $\Phi_\Delta = 0.55$ in $CHCl_3$) as illustrated in Eq. **1** as follows:

$$\Phi_\Delta^S = \Phi_\Delta^{REF} \times \left(\frac{n_S}{n_{REF}}\right)^2 \frac{G_\Delta^S}{G_\Delta^{REF}} \times \frac{A_{REF}}{A_S}, \quad [1]$$

where Φ_Δ denotes the singlet oxygen quantum yield, G_Δ indicates the integrated emission intensity, A represents the absorbance at the operation excitation wavelength, n reflects the solvent's refractive index, given that the SuperScripts *REF* and *S* stand for the reference and sample, respectively. In all cases, we had measured the $^1O_2$ emission spectra upon due excitation. To reduce the impacts of reabsorption of the emitted light, all absorbance was set at 0.05 as well.

Cell Culture. Human HeLa (cervical carcinoma) and WPMY-1 (normal prostate stroma immortalized cell) cells were grown in DMEM; A549 (lung adenoma) were maintained in a mixture of Ham's F-12K medium and L-glutamine (N3520; Sigma); QSG-7701 (normal liver cell), HK-1, and HONE1 (nasopharyngeal carcinoma) were grown in RMPI-1640 medium; MRC-5 (normal lung fibroblasts) and SK-N-SH (neuroblastoma) cells were grown in MEM medium. What were added also are (*i*) 10% (vol/vol) FBS, (*ii*) 100 μg/mL streptomycin, and (*iii*) 100 units/mL penicillin.

In Vitro Imaging. To test the suitability of our water-soluble complexes as bioprobes, we had, using a commercial confocal laser-scanning microscope, Leica TCS SP5, equipped with a Ti:sapphire laser (Libra II; Coherent) as well as a 980-nm wavelength laser for excitation, conducted in vitro imaging of HeLa/WPMY-1/MRC-5 cells with which our five complexes was incubated.

MTT Cell Viability Assay. After 24 h, the water soluble complexes and the targeted cells treated were incubated further with MTT (0.5 mg/mL) for 4 h, so that formazan can be formed along with the cell's metabolic pathways. Then, we had extracted the formazan and dissolved it by dimethyl sulfoxide (DMSO), with the absorbance of the subsequent solutions being measured in a Bio-Rad iMark microplate reader (490 nm). Quadruplicates were performed and we had interpreted and analyzed the data by plottings using the GraphPad Prism 5 software.

PDT Assay. On the 96-well plate, cancer cells (2×10^4 per well) were first incubated overnight and then treated with our complexes and control analogs for the next 6 h in dark. After the old medium was replaced with the the fresh one, the cells were accordingly exposed to yellow light (1–8 J/cm^2) generated from a 400-W tungsten lamp fitted with a heat-isolation filter and a 500-nm long-pass filter under the fluency rate of milliwatts per square centimeter. After that, we had examined the post-PDT cell viability by the MTT assay after 24 h. We had rinsed the cell monolayers with PBS before incubation with 250 μg/mL MTT solution at 37 °C for 3 h. The formazan crystals formed and dissolved in DMSO then underwent absorbance measurement at 540 and 690 nm by a 96-well plate reader (ELx800 Absorbance Microplate Reader).

Animals. We had done all our experiments entailing animal models on the athymic nude mice (BALB/c-nu/nu), which were all obtained from Guangdong Medical Lab Animal Center (license number SCXK-2008-0002). Mice were raised and operated according to the strict protocol the National Standard of Animal Care and Use Procedures (20080820).

Pharmacokinetics analysis. Gd-N and Gd-RhB (1.0 μmol/kg body weight each) were caudal vein injected into the mice. Then sera were collected at different time points from 0 to 20 h as indicated. The concentrations of Gd-N and Gd-RhB were measured by PerkinElmer EnVision Multilabel Reader 2104 at 570 nm, and calculated using standard absorptions via concentration curve. Pharmacokinetic parameters ($t_{1/2}$, V_d, MRT, and area under the concentration–time curve) were calculated by fitting with one compartment model.

In Vivo Biodistribution via ICP-MS. To understand more about the in vivo uptakes of our complexes, biodistribution studies with complexes' specialty to particular organs were carried out via ICP-MS. We administered Gd-N and Gd-RhB to the mice at a dosage of 1.0 μmol/kg body weight when we found that tumor xenograft had attained a size of 0.1 cm^3 approximately. When 2 d passed, around 0.02–0.04 g of sample tissues were collected in tumor, liver, lung, kidney, spleen, brain, prostate, and skin; blood (80–90 μL) is also no

exception. We had incubated all samples with 500 μL of nitric acid at 37 °C for releasing the metal ions for further ICP-MS examinations, in addition to dissolving the interfering organic molecules.

In Vivo PDT Studies. For the establishment of the mouse tumor xenograft mode, cells were to be trypsinized, harvested, and suspended in the culture medium. We had injected 1×10^6 cells in 100 μL volume s.c. into the flanks of female athymic nude mice (5 wk of age) and waited for 10–15 d. When the tumor volume reached the size of 100–150 mm^3, we divided the animals randomly into different groups for further experiments. Tumor volume was measured by calipers (accuracy of 0.02 mm) and then calculated independently on the basis of the equation $V = (L \times W^2)/2$, where L and W correspond to the larger and smaller dimensions, respectively. One-way analysis of variance toward statistical significances between groups was assessed by the GraphPad Prism 5.0 software.

ACKNOWLEDGMENTS. This work was funded by grants from The Hong Kong Research Grants Council [Hong Kong Baptist University (HKBU) 203112], HKBU (FRG 2/12-13/002), and Hong Kong Polytechnic University Projects YL01 and GUCO8. The work was also supported by Partner State Key Laboratory of Environmental and Biological Analysis and the Strategic Development Fund of HKBU.

1. Kamkaew A, et al. (2013) BODIPY dyes in photodynamic therapy. *Chem Soc Rev* 42(1): 77–88.
2. Liang X, Li X, Jing L, Yue X, Dai Z (2014) Theranostic porphyrin dyad nanoparticles for magnetic resonance imaging guided photodynamic therapy. *Biomaterials* 35(24): 6379–6388.
3. Hemmer E, et al. (2013) Upconverting and NIR emitting rare earth based nanostructures for NIR-bioimaging. *Nanoscale* 5(23):11339–11361.
4. Kachynski AV, et al. (2014) Photodynamic therapy by in situ nonlinear photon conversion. *Nat Photonics* 8:455–461.
5. Celli JP, et al. (2010) Imaging and photodynamic therapy: Mechanisms, monitoring, and optimization. *Chem Rev* 110(5):2795–2838.
6. Zhang JX, et al. (2012) A potential water-soluble ytterbium-based porphyrin-cyclen dual bio-probe for Golgi apparatus imaging and photodynamic therapy. *Chem Commun (Camb)* 48(77):9646–9648.
7. Collins HA, et al. (2008) Blood-vessel closure using photosensitizers engineered for two-photon excitation. *Nat Photonics* 2:420–424.
8. Bonneau S, Morlière P, Brault D (2004) Dynamics of interactions of photosensitizers with lipoproteins and membrane-models: Correlation with cellular incorporation and subcellular distribution. *Biochem Pharmacol* 68(7):1443–1452.
9. Zhang JX, et al. (2012) Comparative studies of the cellular uptake, subcellular localization, and cytotoxic and phototoxic antitumor properties of ruthenium(II)-porphyrin conjugates with different linkers. *Bioconjug Chem* 23(8):1623–1638.
10. D'Souza GGM, Wagle MA, Saxena V, Shah A (2011) Approaches for targeting mitochondria in cancer therapy. *Bioenergetics* 1807:689–696.
11. Zhang T, et al. (2013) Fast Uptake, water-soluble, mitochondria-specific erbium complex for dual function molecular probe—imaging and photodynamic therapy. *RSC Adv* 3:382–385.
12. Azenhaa EG, et al. (2002) Heavy-atom effects on metalloporphyrins and polyhalogenated porphyrins. *Chem Phys* 280:177–190.
13. Schmidt R, Afshari E (1990) Comment on "Effect of solvent on the phosphorescence rate constant of singlet molecular oxygen (1.DELTA.g)." *J Phys Chem* 94:4377–4378.
14. Khalil GE, et al. (2007) NIR luminescence of gadolinium porphyrin complexes. *Chem Phys Lett* 435:45–49.
15. Zhang T, et al. (2013) Porphyrin-based ytterbium complexes targeting anionic phospholipid membranes as selective biomarkers for cancer cell imaging. *Chem Commun (Camb)* 49(65):7252–7254.
16. Hinnen P, et al. (1998) Biochemical basis of 5-aminolaevulinic acid-induced protoporphyrin IX accumulation: A study in patients with (pre)malignant lesions of the oesophagus. *Br J Cancer* 78(5):679–682.
17. Idris NM, et al. (2012) In vivo photodynamic therapy using upconversion nanoparticles as remote-controlled nanotransducers. *Nat Med* 18(10):1580–1585.
18. Ferrario A, Rucker N, Wong S, Luna M, Gomer CJ (2007) Survivin, a member of the inhibitor of apoptosis family, is induced by photodynamic therapy and is a target for improving treatment response. *Cancer Res* 67(10):4989–4995.